Aalborg Universitet

AALBORG UNIVERSITY

An Analytical Model for Performance Optimization of Thermoelectric Generator With Temperature Dependent Materials

Qing, Shaowei ; Rezaniakolaei, Alireza; Rosendahl, Lasse Aistrup; Gou, Xiaolong

Published in:
IEEE Access

DOI (link to publication from Publisher):
10.1109/ACCESS.2018.2874947

Publication date:
2018

Document Version
Publisher's PDF, also known as Version of record

Link to publication from Aalborg University

Citation for published version (APA):
Qing, S., Rezaniakolaei, A., Rosendahl, L. A., & Gou, X. (2018). An Analytical Model for Performance Optimization of Thermoelectric Generator With Temperature Dependent Materials. *IEEE Access*, *6*, 60852-60861. Article 8487047. https://doi.org/10.1109/ACCESS.2018.2874947

General rights
Copyright and moral rights for the publications made accessible in the public portal are retained by the authors and/or other copyright owners and it is a condition of accessing publications that users recognise and abide by the legal requirements associated with these rights.

- Users may download and print one copy of any publication from the public portal for the purpose of private study or research.
- You may not further distribute the material or use it for any profit-making activity or commercial gain
- You may freely distribute the URL identifying the publication in the public portal -

Take down policy
If you believe that this document breaches copyright please contact us at vbn@aub.aau.dk providing details, and we will remove access to the work immediately and investigate your claim.

Downloaded from vbn.aau.dk on: May 04, 2026

IEEE Access
Multidisciplinary | Rapid Review | Open Access Journal

Received August 10, 2018, accepted September 28, 2018, date of publication October 9, 2018, date of current version November 9, 2018.

Digital Object Identifier 10.1109/ACCESS.2018.2874947

An Analytical Model for Performance Optimization of Thermoelectric Generator With Temperature Dependent Materials

SHAOWEI QING[1,2], ALIREZA REZANIAKOLAEI[3], LASSE A. ROSENDAHL[3], (Senior Member, IEEE), AND XIAOLONG GOU[1,2]

[1]Key Laboratory of Low-Grade Energy Utilization Technology and System, Ministry of Education, Chongqing University, Chongqing 400044, China
[2]Department of Energy and Power Engineering, Chongqing University, Chongqing 400044, China
[3]Department of Energy Technology, Aalborg University, 9220 Aalborg, Denmark

Corresponding author: Shaowei Qing (qshaowei@cqu.edu.cn)

This work was supported in part by the National Natural Science Foundation of China under Grant 11605018 and Grant 51776023, and in part by the Fundamental Research Funds for the Central Universities under Grant 0233005202049.

ABSTRACT Accurate and efficient performance prediction of thermoelectric generators (TEG) is important for integrated and multi-parameter optimization especially in large-scale energy harvesting applications. In this paper, a comprehensive analytical model coupled with non-identical temperature-dependent material properties and effective heat transfer coefficient (EHTC) of both-sides heat exchangers is built to investigate the internal and external characteristics of the TEG. Parametric optimization of the TEG is carried out to maximize the output power and efficiency over a wide range of EHTCs, fill factor, and geometry of thermoelectric (TE) elements. The developed model can be efficiently solved by function solver (i.e. fsolve) in Matlab software, and its accuracy is validated with previous multi-physics numerical TEG model. The results show that statistical parameters of the TE element present non-linear behavior with variation of electrical load resistance. The optimal load ratio is larger than unit, and it reduces monotonically with increment of the cold-side EHTC, but changes inversely with the hot-side EHTC. For a fixed sum value of both-sides EHTCs, there are two different optimal ratios of the hot-side EHTC to the cold-side EHTC for maximum efficiency and power. In addition, the optimal length and cross-sectional area ratio of the TE elements are investigated with detailed analysis.

INDEX TERMS Thermoelectric generator, parametric optimization, thermal reservoirs, temperature-dependent materials.

I. INTRODUCTION

Due to the world-wide increasingly serious problems of energy shortage and environment pollution, there is a growing interest in applying novel technologies to maximize the total utilization efficiency of energy systems [1]. Thermoelectric generator (TEG) is a promising method which can directly convert thermal energy into electricity without any moving parts, and thus it has great application potential in industrial energy systems to harvest the large amount of waste heat [2]–[4].

In order to obtain maximum output power and efficiency, one tends to select high-performance heat exchangers with large heat transfer coefficient and thermoelectric (TE) materials with high dimensionless figure-of-merit (ZT). Another method is to improve the way where existing TEGs are currently used [2]. For the latter method, the output power of the TEG needs to be predictable. The performance of TE modules for different applications such as hybrid systems [5]–[7], automotive [8], [9], data centers [10], human body [11], geothermal [12], solar [13]–[15], spacing [16], and for different type of TEGs such as one TE panel and multi TE panels [17]–[19], in series and parallel [20], [21], helical and linear structures [22], [23], has been modelled.

2169-3536 © 2018 IEEE. Translations and content mining are permitted for academic research only.
Personal use is also permitted, but republication/redistribution requires IEEE permission.
See http://www.ieee.org/publications_standards/publications/rights/index.html for more information.

In fact, there are many design parameters such as thermoelement lengths (L_p, L_n) and footprint areas (A_p, A_n) of p-type and n-type TE elements and heat exchangers that can significantly influence the performance of the TEG system. Rowe and Min [24] showed that the thermoelement length plays an important role in the power generation. Yilbas and Sahin [25] found that there is an optimal slenderness ratio $X_{opt} = (A_p/L_p)/(A_n/L_n)$ to maximize efficiency of the TEG. Moreover, Yazawa and Shakouri [26] found that the optimal internal parameters of the TEG module such as thermal conductivity of TE element are strongly correlated with the external parameters, e.g. the load ratio and the sum of external thermal resistances. It has been gradually recognized that the co-design optimization including the geometry of TE elements and the heat exchangers is critical for achieving maximum output power and efficiency.

Some analytical and numerical models were developed to optimize geometry of the TE elements and heat exchangers, nevertheless approximations of the critical parameters and assumptions such as the identical materials and temperature-independent properties of TE elements were used in these studies [27]–[32]. With the assumption of identical materials, it is found that the predictions of TEG numerical model under constant material properties differ much with that of temperature-dependent varying material properties [33]. The thermoelectric properties such as Seebeck coefficient, electrical conductivity and thermal conductivity of p- and n-type TE elements are not identical and are temperature dependent, so that cause different temperature distribution and thermal-electrical behavior in the TE elements [34]. Zhang [35] proposed a one-dimensional model by giving the nonlinear analytical solution of heat conduction equation and using control volume method to predict the optimal parameters (e.g. fill factor) of TEG with temperature-dependent material properties. Barry *et al.* [36] developed aone-dimensional analytical model combined with complete thermal resistance network to optimize the geometry of TE elements, and found that performance of the TEG can be significantly improved by geometric optimization. Shen *et al.* [37] developed a comprehensive one-dimensional steady-state theoretical model to stress the side surface heat transfer (SSHT) with the assumption that the end temperature of p-type element equals to that of n-type. Manikandan and Kaushik [38] built a thermodynamic model to study the influence of the Thomson effect on the performance optimization of two-stage TEG. Feng *et al.* [39], [40] studied the Thomson effect on the performance of a TEG-driven heat pump combined device and a TEG-TEC device. Wu *et al.* [41] built a device-level theoretical model to study the influence of contact thermal resistance, the Thompson effect, the Joule heat and heat leakage on the TEG performance. Chen *et al.* [42] proposed a one dimensional numerical model which can deal with the temperature-dependent material properties with an assumption that the end temperature of p-type element equals to that of n-type. They, furthermore, developed a three-dimensional model implemented in a computational fluid dynamics (CFD) simulation environment [43]. This model can be conveniently connected to various CFD models of heat sources as a continuum domain to conduct co-design optimization of the TEG system [44]. Rezania *et al.* [45] developed a three-dimensional uni-couple model with different heat transfer coefficient imposed on the cold junction. They used finite element method to solve this model, and found an optimal ration forA_n/A_p to achieve maximum output power. Using a three-dimensional multi-physics TEG model, Meng *et al.* [46] proposed a multi-parameters optimization method, including optimal uni-couple number, footprint length and fill factor, to obtain maximum output power, with an assumption that the p-type and n-type TE element have same properties and geometry. Niu *et al.* [47] developed three-dimensional numerical models including temperature-dependent material properties to predict the heat and electrical transfer in the TEG, and found that changing the shape of TE element from normal cuboid (constant cross-sectional area) to hexahedrons (variable cross-sectional area) could increase the power output significantly. Erturun *et al.* [48] found that both width and height of TE element have a significant effect on power generation and thermal stresses, by using statistical and finite-element methods. Högblom and Andersson [49] proposed a novel model allowing the heat flow coupled with the electric current in a large system of modules, in which the thermal model allows for a two-way coupling in CFD analysis.

As mentioned above, many analytical and numerical models were built to optimize the parameters of TEG system. In general, these parameters include the geometry of p-type (A_p, L_p) and n-type (A_n, L_n) elements, the fill factor, the load resistance (which is usually used as virtual load in maximum power point tracking algorithm [50], but is treated as equivalent heating resistance in this study) and the geometry of typical heat exchangers at the hot and cold sides of the TEG, which means a great deal of time expense. In this case, the analytical model based on assumptions of identical material and temperature-independent material properties is very convenient to optimize a TEG system [27], [28], however these assumptions obviously degrade the accuracy [33]. Conversely, the three-dimensional numerical model including temperature-dependent material properties and almost all the multi-physics processes can obtain higher accuracy, but the time expense is significantly larger [33], [43]–[49].

Therefore, it is necessary to develop an accurate and efficient model for multi-parameter optimization of TEG. In this study, a fully coupled 1-D analytical TEG model is built. The temperature-dependent properties such as Seebeck coefficient, electrical resistivity and thermal conductivity of TE materials, the thermal resistances of ceramic substrate and heat exchanger corresponding to p-type and n-type TE elements, and the junction temperatures of p-type and n-type TE elements at hot side (T_{1p}, T_{1n}) and cold side (T_{2p}, T_{2n}) as well as the geometry of p-type (A_p, L_p) and n-type (A_n, L_n) TE elements are considered. A wide range of effective heat transfer coefficient is imposed on the hot side (h_h) and cold

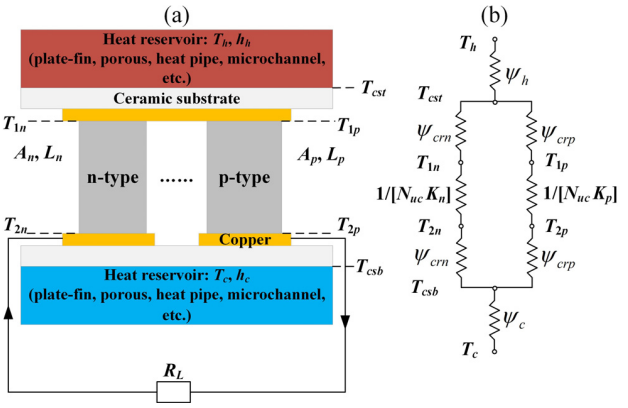

FIGURE 1. (a) Schematic sandwich diagram of TEG; (b) thermal resistance network for TEG: corresponding to p-type TE elements (right side) and n-type (left side).

side (h_c) to study the internal and external characteristic variation in the TEG. The proposed model is validated to have comparable accuracy in comparison to three-dimensional numerical models.

This paper is organized as follows: The governing analytical TEG model is described in Section 2. The developed analytical model is validated in Section 3. Section 4 presents discussions and results with detailed parametric analysis to reveal the internal and external characteristics of the TEG. Conclusions are given in Section 5.

II. MODELLING

The typical schematic of TEG is shown in Fig. 1. In this study, N_{uc} uni-couples are connected electrically in series and thermally in parallel between two dielectric ceramic plates to form the TEG module. Optimal junction temperatures at the hot side of the p-type and n-type TE elements (T_{1p}, T_{1n}) and at the cold side of the elements (T_{2p}, T_{2n}) and the optimal geometric parameters such as footprint areas (A_p, A_n) and lengths (L_p, L_n) of the TE elements are not identical. The material properties such as Seebeck coefficient ($\alpha_p(T)$, $\alpha_n(T)$), electrical resistivity ($\rho_p(T)$, $\rho_n(T)$) and thermal conductivity ($k_p(T)$, $k_n(T)$) [25], [26], [45] are temperature dependent. The fill factor of the TE elements is defined as:

$$F = N_{uc}\left(A_p + A_n\right)/A_{total} \tag{1}$$

where, A_{total}=$W\times L$ is the area of ceramic substrate.

Temperatures at the hot and cold reservoirs are fixed as T_h and T_c, respectively.

A. GOVERNING EQUATIONS

The average Seebeck coefficient of the uni-couple is:

$$\begin{aligned}\bar{\alpha} &= \bar{\alpha}_p - \bar{\alpha}_n \\ &= \frac{1}{T_{1p}-T_{2p}}\int_{T_{2p}}^{T_{1p}} \alpha_p dT_p - \frac{1}{T_{1n}-T_{2n}}\int_{T_{2n}}^{T_{1n}} \alpha_n dT_n\end{aligned} \tag{2}$$

where, $\bar{\alpha}_p$ and $\bar{\alpha}_n$ are, respectively, the average Seebeck coefficient of p- and n-type TE elements.

The temperature dependent electrical resistance and thermal conductance of the p- and n-type TE elements are [42]:

$$R_{p,n} = \int_0^{L_{p,n}} \frac{\rho_{p,n}\left(T_{p,n}(x)\right)}{A_{p,n}} dx \tag{3a}$$

$$K_{p,n} = \frac{1}{\int_0^{L_{p,n}} dx \Big/ \left[k_{p,n}\left(T(x)\right) A_{p,n}\right]} \tag{3b}$$

Based on the three-dimensional numerical results, the temperature through the TE elements approximately obeys linear distribution [33]. Therefore, with the assumption of linear temperature distribution along TE elements, (3a) and (3b) become:

$$R_{p,n} = \frac{L_{p,n}}{A_{p,n}} \frac{1}{T_{1p,n}-T_{2p,n}} \int_{T_{2p,n}}^{T_{1p,n}} \rho_{p,n} dT = \frac{L_{p,n}}{A_{p,n}} \bar{\rho}_{p,n} \tag{4a}$$

$$K_{p,n} = \frac{A_{p,n}}{L_{p,n}} \frac{1}{\frac{1}{T_{1p,n}-T_{2p,n}} \int_{T_{2p,n}}^{T_{1p,n}} \frac{1}{k_{p,n}} dT} = \frac{A_{p,n}}{L_{p,n}} \frac{1}{\bar{r}_{p,n}} \tag{4b}$$

where, $\bar{\rho}_{p,n}$ and $\bar{r}_{p,n}$ are the average electrical resistivity (Ωm) and average thermal resistivity (mK/W) of the p- and n-type TE elements respectively. Therefore, the total internal resistance of the TEG module is $R = N_{uc}(R_p + R_n)$.

Consequently, circuit current of the TEG is as follows:

$$\begin{aligned} I &= \frac{U}{R + R_L} \\ &= \frac{N_{uc}\left[\bar{\alpha}_p\left(T_{1p}-T_{2p}\right) - \bar{\alpha}_n\left(T_{1n}-T_{2n}\right)\right]}{R\left(1+m\right)} \end{aligned} \tag{5}$$

And the output power and efficiency of the TEG are [26]:

$$\begin{aligned} w &= I^2 mR = N_{uc}^2 \frac{m}{R\left(1+m\right)^2} \\ &\quad \times \left[\bar{\alpha}_p\left(T_{1p}-T_{2p}\right) - \bar{\alpha}_n\left(T_{1n}-T_{2n}\right)\right]^2 \end{aligned} \tag{6a}$$

$$\eta = \frac{w}{Q_h} \tag{6b}$$

where, U is total electric voltage, and $m = R_L/R$ is resistance ratio. The underload voltage is $U_{out} = IR_L$. In (6b), Q_h is the total heat flux transferred from the hot reservoir to the TE module.

B. THERMAL RESISTANCES NETWORK OF THE TEG

The thermal resistance network for the TEG is shown in Fig. 1(b). For simplicity, electrical and thermal contact resistances between module layers are neglected. The copper interconnectors have high thermal conductivity in comparison to that of ceramic substrate and TE elements, therefore, the thermal resistance of the interconnectors can be neglected in this study.

For thermal resistance of the ceramic substrate, since $F<1$, the total heat dissipation area A_{total} of the ceramic substrate is geometrically divided into a "gap" heat dissipation area, $A_{gap}=(1-F)A_{total}$, and correspondingly an "occupied" heat dissipation area, $A_{occupied}=FA_{total}=N_{uc}(A_p+A_n)$. The spreading thermal resistance at the "gap" area reduces the heat flow cross-section area. According to [26] and [51], the total thermal resistances of the ceramic substrate corresponding to the p-and n-type TE elements are:

$$\psi_{crp,n}=\frac{\lambda_{crp,n}}{N_{uc}k_{cr}\left(1+2\lambda_{crp,n}\tan\Phi_{crp,n}\right)\sqrt{A_{p,n}}} \tag{7}$$

where,

$$\Phi_{crp,n}=5.86\ln\left(\lambda_{crp,n}\right)+40.4\ 0.0011<\lambda_{crp,n}<1$$
$$\Phi_{crp,n}=46.45-6.048\lambda_{crp,n}^{-0.969}\ \lambda_{crp,n}\geq 1,$$

$\lambda_{crp,n}=t_{cr}/\sqrt{A_{p,n}}$, and k_{cr} and t_{cr} are the thermal conductivity and depth of the ceramic substrate, respectively.

For the hot side and cold side heat reservoirs, the total thermal resistances are:

$$\psi_h=1/(h_hA_{total}),\quad \psi_c=1/(h_cA_{total}) \tag{8}$$

where, the unit of h_h and h_c is W/K per m^2 of ceramic substrate.

C. ENERGY BALANCE AT THE INTERFACE BETWEEN HEAT RESERVOIRS AND CERAMIC SUBSTRATES

At the interface between the hot-side heat reservoir and ceramic substrate, the thermal flux is:

$$Q_h=\frac{(T_h-T_{cst})}{\psi_h}=Q_{hp}+Q_{hn} \tag{9}$$

where, $Q_{hp}=\left(T_{cst}-T_{1p}\right)/\psi_{crp}$ and $Q_{hn}=(T_{cst}-T_{1n})/\psi_{crn}$ are the total thermal flux from the hot-side ceramic substrate to the p and n-type TE elements, respectively.

At the interface between the cold-side ceramic substrate and heat reservoir, the thermal flux is:

$$Q_c=\frac{(T_{csb}-T_c)}{\psi_c}=Q_{cp}+Q_{cn} \tag{10}$$

where, $Q_{cp}=\left(T_{2p}-T_{csb}\right)/\psi_{crp}$ and $Q_{cn}=(T_{2n}-T_{csb})/\psi_{crn}$ are the total thermal flux from p and n-type TE elements to cold-side ceramic substrate respectively.

D. ENERGY BALANCE FOR COLD AND HOT JUNCTIONS OF TE ELEMENTS

By taking thermal energy conversation at the cold and hot junctions of the TE elements [26], [28], the heat transfer at hot and cold junctions of the p-type TE elements are as follows:

$$Q_{hp}=N_{uc}\left[\bar{\alpha}_pIT_{1p}+K_p(T_{1p}-T_{2p})-I^2R_p/2\right]=\frac{\left(T_{cst}-T_{1p}\right)}{\psi_{crp}} \tag{11a}$$

TABLE 1. Comparisons of analytical and numerical results.

Quantity	present results	Meng *et al.*'s results[33]	Chen *et al.*'s results[43]
Q_h (W)	78.3	81.2	81.8
w (W)	3.45	3.88	3.62
I (A)	1.01	1.08	1.032
η (%)	4.41	4.77	4.43

$$Q_{cp}=N_{uc}\left[\bar{\alpha}_pIT_{2P}+K_p(T_{1p}-T_{2p})+I^2R_p/2\right]=\frac{\left(T_{2p}-T_{csb}\right)}{\psi_{crp}} \tag{11b}$$

And the heat transfer at hot and cold junctions of the n-type TE elements are:

$$Q_{hn}=N_{uc}\left[-\bar{\alpha}_nIT_{1n}+K_n(T_{1n}-T_{2n})-I^2R_n/2\right]=\frac{(T_{cst}-T_{1n})}{\psi_{crn}} \tag{12a}$$

$$Q_{cn}=N_{uc}\left[-\bar{\alpha}_nIT_{2n}+K_n(T_{1n}-T_{2n})+I^2R_n/2\right]=\frac{(T_{2n}-T_{csb})}{\psi_{crn}} \tag{12b}$$

By solving (9)-(12b) combined with auxiliary (2), (2)-(8), the effect of critical design parameters on the performance of TEG can be analyzed over wide range of h_h and h_c.

III. MODEL VALIDATION: THE ACCURACY AND COMPUTATIONAL EFFICIENCY

In order to check validation of the developed model, the results of this study are compared with previous literatures. All the geometrical dimensions and physical parameters are taken the same as multi-physics field numerical models by Meng *et al.* [33] and Chen *et al.* [43] with the TEG hot and cold conjunctions' temperature at 423 K and 303 K, respectively. The thermal conductivity and the thickness of the ceramic substrate are taken k_{cr}=130 W/K/m and $t_{cr}=0.2$ mm, respectively. The length of the temperature dependent TE elements is $L_p=L_n$=1.6 mm for a cross-sectional area of $A_p=A_n$=1.4×1.4 mm^2.

Under conditions above, Q_h, w, I and η can be predicted by the three models and measurement, as shown in Table 1. As Table 1 shows, Q_h and I of present model are very close (i.e. almost all the deviations are lower than 5 %) to results from Meng *et al.* and Chen *et al.*; although w and η of present model are respectively 11.08 % and 7.55 % lower than results of Meng *et al.*, they are respectively 4.7 % and 0.45 % lower than results of Chen *et al.* Therefore, the present model can approximately offer accurate results in comparison to the three-dimensional numerical models.

In the present analytical model, only 6 unknown parameters, i.e. T_{1p}, T_{1n}, T_{2p}, T_{2n}, T_{cst} and T_{csb} in (9)-(12b) need to be solved. As a steady-state, 1-D thermoelectric conversion problem, the 6 equations associated with the auxiliary equations (1)-(8) can be solved easily by function solver,

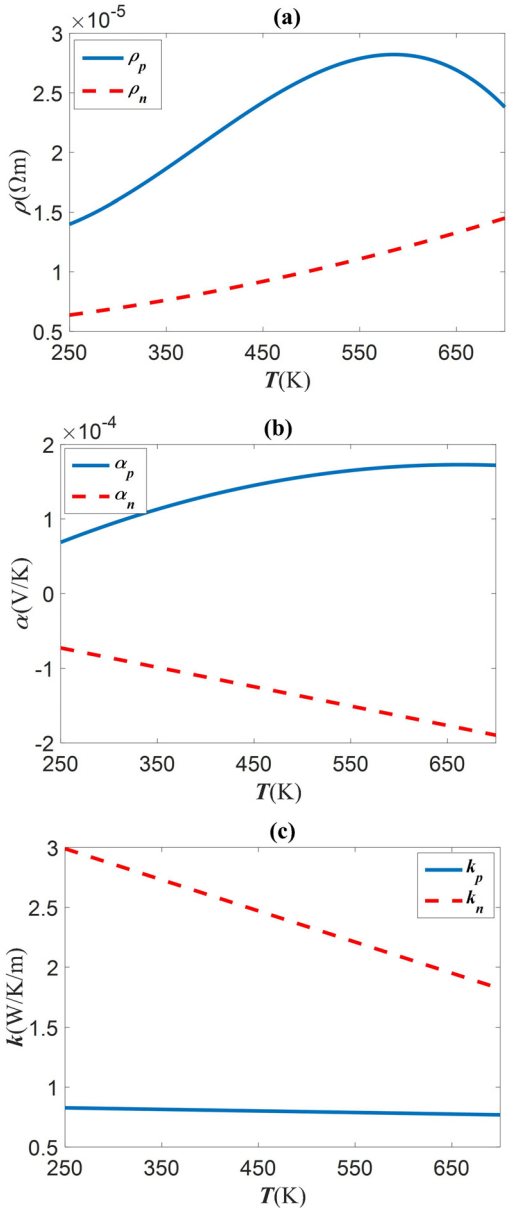

FIGURE 2. Thermoelectric properties of p-type (Zn_4Sb_3) [52] and n-type ($Mg_2Si_{1-x}Sn_x$) [53] TE materials. (a) electrical resistivity, ρ; (b) Seebeck coefficient, α; (c) thermal conductivity, k.

namely "fsolve" in Matlab software. The solver is very efficient, and the calculated accuracy can be self-validated by checking errors of the 6 equations. Therefore, the present model is more efficient for performance prediction of the TEG, in comparison with three-dimensional multi-physics numerical models which need to solve the three-dimensional temperature distribution of each TE element.

IV. RESULTS AND DISCUSSIONS

In this study, the TEG substrate area is $W \times L$=4 cm×4 cm. Fig. 2 shows the non-identical and temperature-dependent thermoelectric properties of the p- and n-type materials, Zn_4Sb_3 [52] and $Mg_2Si_{1-x}Sn_x$ [53] respectively, used in this study. The total area of the p- and n-footprints (A_p+A_n)

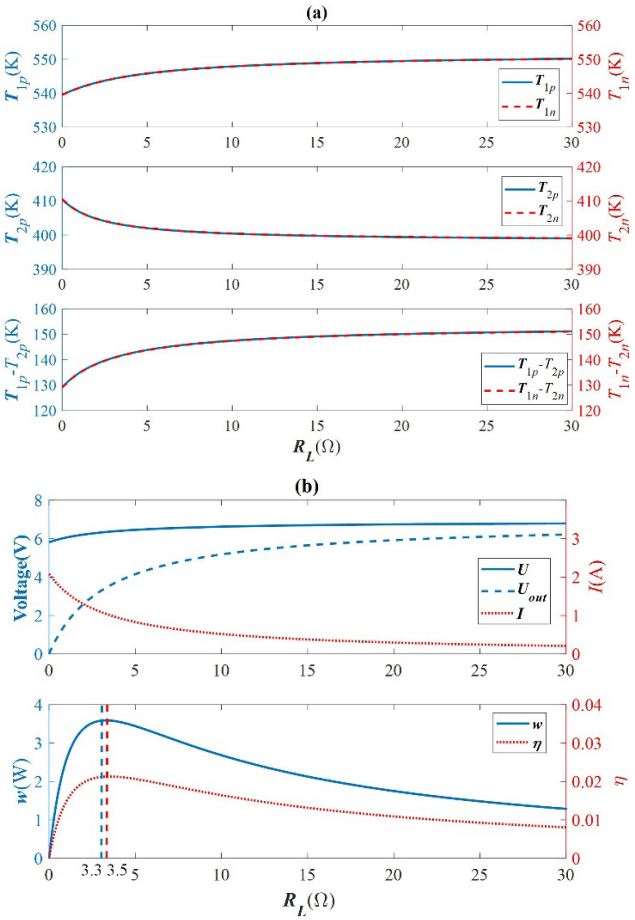

FIGURE 3. Effect of R_L on (a) T_{1p} and T_{1n}, T_{2p} and T_{2n}, temperature differences $T_{1p} - T_{2p}$ and $T_{1n} - T_{2n}$; (b) U, U_{out}, I, w and η.

is fixed at 8 mm^2. The ceramic substrate is made of Alumina with thermal conductivity of 30 W/K/m and thickness of t_{cr}=10 μm. Below, for a specific calculation, normally following parameters are used: N_{uc}=160, $F = 0.8$, $A_p = A_n$, $L_p = L_n = 2$ mm, $T_h = 650$ K, $T_c = 300$ K, $h_h = h_c = 1000$ W/K/m^2.

A. KEY PARAMETERS VARIATION VERSUS LOAD RESISTANCE

In order to show impact of thermoelectric properties of the TE elements on the system performance, the cross sectional area and TE elements length are taken equal, i.e. $A_p = A_n$, $L_p = L_n$, which gives $\psi_{crp} = \psi_{crn}$ based on (7). Moreover, due to $k_n \approx 3k_p$ in Fig. 2(c), the thermal conductance of n-type would be much bigger than that of n-type based on (4b), i.e. $K_n \approx 3K_p$, which indicates that Q_{hn} should be much bigger than Q_{hp}. However, the junction temperatures of n-type TE element (T_{1p} and T_{2p}) are very close to that of p-type TE element (T_{1n} and T_{2n}), due to the thermal resistances of ceramic substrate corresponding to n- and p-type TE elements (ψ_{crn} and ψ_{crp}) are very small.

Indeed, as shown in Fig. 3(a), the junction temperatures of p- and n-type TE elements are very close. Moreover, one

can see that variation of the load resistance R_L influences the junction temperatures of TE element dramatically. It needs to point out that, $K_p, K_n, R_p, R_n, \bar{\alpha}$ and so on vary slightly with increment of R_L, while the circuit current, I, reduces significantly with increment of R_L (see Fig. 3(b)). For this reason, the Joule heat term $I^2R_p/2$ in (11a) decreases which tends to increase Q_{hp}, but the decrement of Peltier heat term $\bar{\alpha}_{1p}IT_{1p}$ in (11a) tends to decrease Q_{hp}. We found that the latter tendency is dominant, i.e. Q_{hp} decreases with the increments of R_L, leading toT_{1p} increases with the increment of R_L based on (11a), as shown in Fig. 3(a); for the same reason, T_{1n} also increases with the increasing of R_L. Similarly, due to the electric current Idecreases remarkably with the increasing of R_L (see Fig.3 (d)), both T_{2p} and T_{2n} would decrease according to (11b) and (12b).

Due to variation of the junctions' temperatures in Fig. 3(a), the total open circuit voltage U increases with the R_L, leading to increment of underload voltage $U_{out} = UR_L/(R + R_L)$, as shown in Fig. 3(b). Since the increasing rate of U is lower than unit (i.e. dU/dR_L <1 V/Ω), the electric current I decreases with the increasing of R_L based on (5), as shown in Fig. 3(b). Therefore, due to the inverse variety of U_{out} and I, the output power w and efficiency η present non-monotonic variety. It is worthy to note that there are two optimal load resistances corresponding to maximum output power w_{max} (R_{Lopt}=3.3 Ω) and maximum conversion efficiency η_{max} (R_{Lopt}=3.5 Ω).

B. EFFECT OF HEAT TRANSFER COEFFICIENT ON SYSTEM PERFORMANCE

As shown in Fig. 4(a), the temperature differences across the TE elements enhance as the h_h and h_c increase, which causes that the internal electrical resistance R varies with the heat transfer coefficients, and, therefore, the optimal resistance ratio m_{opt} changes, Fig. 4(b). According to (6a), (6b) and variation of U, R and m_{opt}, the results show that the maximum output power and the corresponding efficiency enhance with increment of h_h and h_c.

Hendricks *et al.* [4] predict that the optimal resistance ratio m_{opt} should be slightly higher than unit. In this paper, the results of this study reveal optimal values of m_{opt} for maximizing the output power. When $m = m_{opt} = R_{Lopt}/R$, $\partial w/\partial m = 0$ (see Fig. 3(b)); $\partial(T_{1p} - T_{2p})/\partial m \neq 0$, $\partial(T_{1n} - T_{2n})/\partial m \neq 0$ (see Fig. 3(a)), $\partial U/\partial m \neq 0$ (see Fig. 3(b)); and $\partial R/\partial m \approx 0$ according to (4a) and Fig. 2(a) and 3(a). Therefore, by taking the above characteristics into the equation of output power, i.e. (6a), the optimal load ratio can be modified as follows:

$$m_{opt} = 1 + 2m_{opt}\left(1 + m_{opt}\right)\left[\frac{1}{U}\frac{\partial U}{\partial m}\right]\Bigg|_{m=m_{opt}} \quad (13)$$

Since $\partial U/\partial m > 0$ (see Fig. 3(b)), m_{opt} would be larger than unit. As a function, m_{opt} can be re-written as:

$$f\left(m_{opt}\right) = \frac{m_{opt} - 1}{2m_{opt}\left(1 + m_{opt}\right)} = \left[\frac{1}{U}\frac{\partial U}{\partial m}\right]\Bigg|_{m=m_{opt}} = C \quad (14)$$

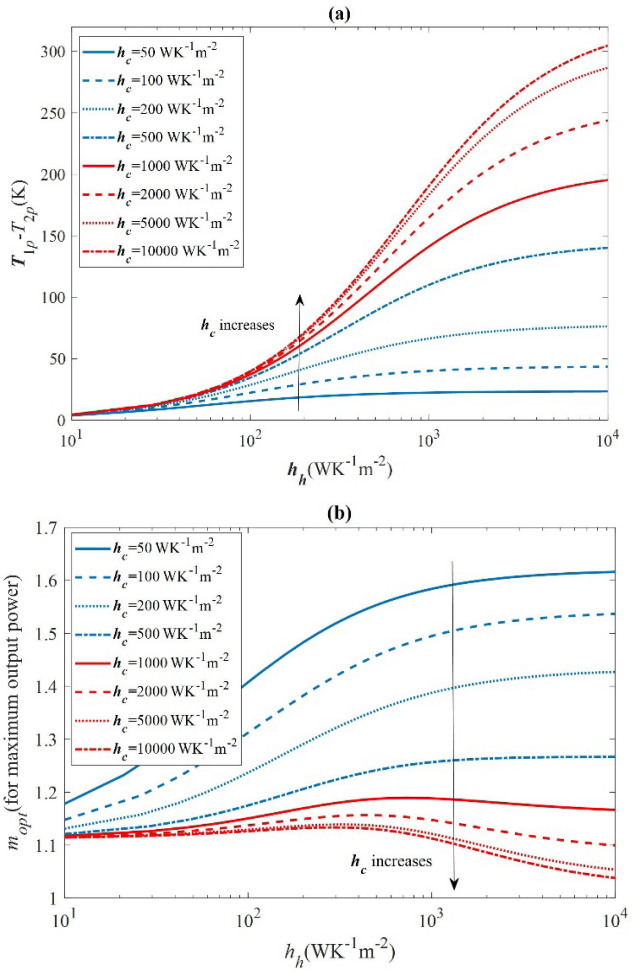

FIGURE 4. Effect of h_h and h_c on TEG performance: (a) temperature difference through p-type TE element; (b) optimal resistance ratio m_{opt}.

where, $f(m_{opt})$ is an increasing function related to m_{opt}. Therefore, m_{opt} varies proportionally with $C = [(\partial U/\partial m)/U]|_{m=m_{opt}}$.

As h_c increases, U enhances significantly, but $\partial U/\partial m|_{m=m_{opt}}$ is a small value (≈(6.36−5.81)/1= 0.55 according to Fig. 3(b)), consequently, C decreases. Thus, m_{opt} decreases monotonically with increment of h_c, as shown in Fig. 4(b).

As h_h increases, U increases too. When $h_c \leq$ 500 W/K/m^2, m_{opt} increases monotonically with h_h, because increment of $\partial U/\partial m|_{m=m_{opt}}$ is greater than that of $U|_{m=m_{opt}}$ with increment of h_h. On the contrary, when $h_c >$ 500 W/K/m^2 and $h_h >$ 150 W/K/m^2 (in this study) m_{opt} decreases with increment of h_h because the increasing rate of $\partial U/\partial m|_{m=m_{opt}}$ is smaller than that of $U|_{m=m_{opt}}$. For high h_c, m_{opt} has a peak value at h_h ≈150 W/K/m^2.

C. OPTIMAL HEAT TRANSFER COEFFICIENT RATIO FOR MAXIMUM PERFORMANCE

The maximum output power in thermoelectric system can be enhanced by using more powerful heat exchangers with higher heat transfer coefficient. However, former literatures

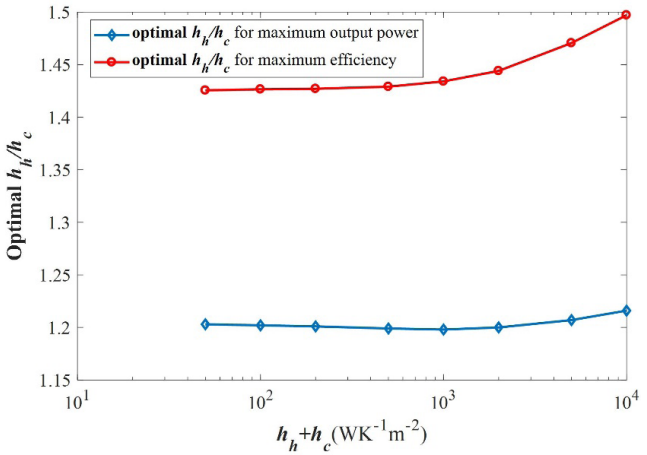

FIGURE 5. Optimal h_h/h_c for maximum efficiency and output power versus $h_h + h_c$.

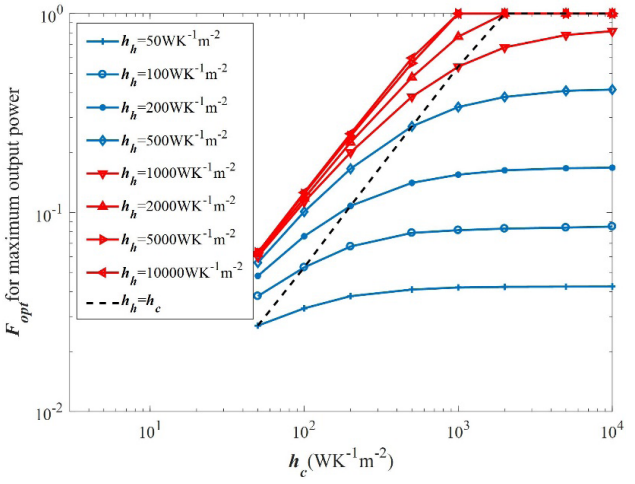

FIGURE 6. Optimal fill factor with heat transfer coefficients for maximum output power.

indicate that the cost of heat exchanger is proportional to heat transfer coefficient [54]–[56], and thus there is an optimal value of h_h+h_c to achieve maximum cost performance ($/W). This section considers optimal ratio of effective heat transfer coefficient for a given value of $h_h + h_c$, in order to obtain maximum output power or efficiency.

As shown in Fig. 5, the optimal ratio of h_h/h_c for maximum conversion efficiency and power generation increases as the $h_h + h_c$ increases. For a given value of $h_h + h_c$, as h_h/h_c increases, the heat transferred to the TEG's hot junction, i.e. $Q_h = Q_{hp}+Q_{hn}$ increases at first due to h_h increases, but then decreases due to T_{1p} and T_{1n} rise and h_c decreases. After the optimal ratio of the h_h/h_c that gives the maximum w_{max} for a constant $h_h + h_c$, Q_h decreases with higher rate than the w_{max}, leading to increment of η based on (6b). Therefore, the optimal ratio of h_h/h_c for η_{max} is higher than that for w_{max}.

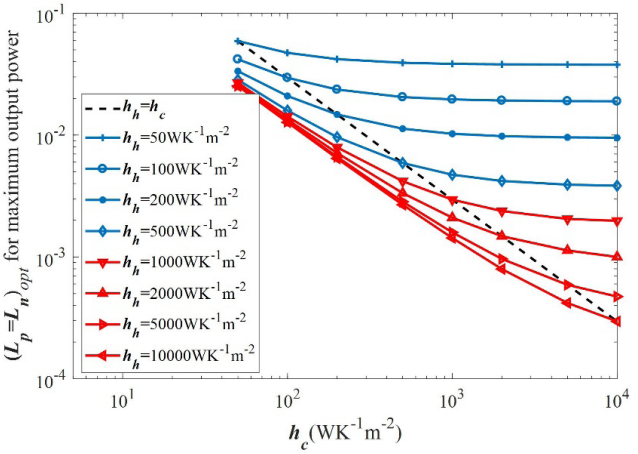

FIGURE 7. Optimal TE element length for maximum output power.

D. OPTIMAL FILL FACTOR FOR MAXIMUM POWER GENERATION

Since the cross sectional area of the TE elements is constant in this study, number of uni-couple, N_{uc}, varies proportionally with the fill factor, F, and the junction temperatures at hot junction (T_{1p}, T_{1n}) of p- and n-type TE elements decrease for given thermal boundary conditions discussed in (11a) and (12b). Furthermore, the junction temperatures at cold junction (T_{2p}, T_{2n}) of p- and n-type TE elements increase, leading to reduction of η_{max} according to (6b) and the classic TE theory [57].

The optimal fill factor F_{opt} for maximum output power is shown in Fig. 6. At low heat transfer coefficients, temperature differences between the cold and hot junctions of the TE elements, $(T_{1p} - T_{2p})$ and $(T_{1n} - T_{2n})$, decrease significantly with the increment of F. Therefore, a smaller value of F is required to provide the optimal temperature difference for the maximum output power. While at high heat transfer coefficients, $h_h = h_c \geq 2000$ W/K/m^2 in this study, $(T_{1p} - T_{2p})$ and $(T_{1n} - T_{2n})$ is less sensitive to variation of the F and a higher value of the F is required to maximize output power by enhancing the heat transferred across the TE elements. Therefore, F_{opt} increases monotonically with the increasing of h_h and h_c.

For the special case (i.e. $h_h = h_c$, the black line in Fig. 6), F_{opt} increases linearly with the increasing of h_h and h_c before reaching unit.

E. OPTIMAL LENGTH OF TE ELEMENTS COUPLED WITH HEAT RESERVOIRS

When the length of TE elements ($L_p = L_n$) increases, the temperature differences across p- $(T_{1p} - T_{2p})$ and n-type $(T_{1n} - T_{2n})$ TE elements enhance, leading to increment of η_{max} according to (6) and the classic TE theory [57].

As the $L_p = L_n$ increases, $\left[\bar{\alpha}_p\left(T_{1p}-T_{2p}\right)-\bar{\alpha}_n\left(T_{1n}-T_{2n}\right)\right]$ in (6a) enhances. On the other hand the internal resistance R in (6a) approximately proportionally increases with length of the TE elements. Therefore, the maximum output power presents a parabolic behaviour with increment of TE element length.

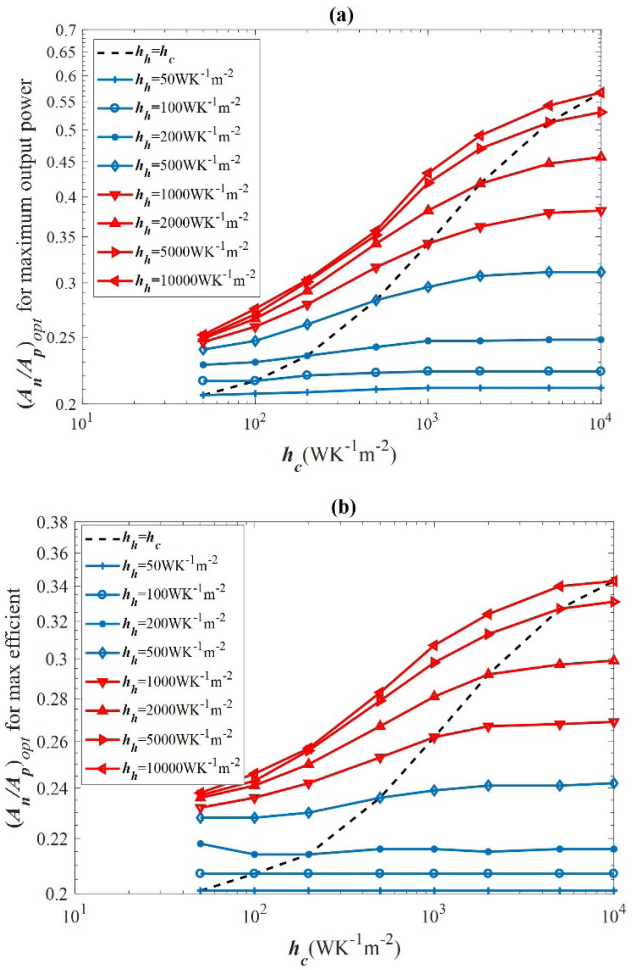

FIGURE 8. (a) Optimal cross-section area ratio for maximum output power; (b) optimal cross-section area ratio for maximum efficiency.

The optimal TE element length $(L_p = L_n)_{opt}$ for maximum output power is shown in Fig. 7. For fixed h_h, the optimum length decreases monotonically with increment of h_c. Furthermore, for a fixed h_c, the optimal length decreases monotonically with increment of h_h. For the special case (i.e. $h_h = h_c$, the black line in Fig. 7, $(L_p = L_n)_{opt}$ has approximately a hyperbolic trend with variation of h_h and h_c.

F. OPTIMAL CROSS-SECTION AREA RATIO COUPLED WITH HEAT TRANSFER COEFFICIENTS

According to classic TE theory [25], [57], there is an optimal slenderness ratio of p-type TE element to n-type, i.e. $X_{opt} = (A_p/L_p)/(A_n/L_n)$ to obtain maximum system efficiency.

In general, when A_n/A_p increases from a very small value (e.g. 10^{-2}), T_{1n} tends to reduce because of the corresponding total heat conduction area of n-type TE elements increases. Moreover, the junction temperature at cold junction of the n-type TE element increases. Therefore, the temperature difference through n-type TE element $(T_{1n} - T_{2n})$ reduces. Conversely, the temperature difference across the p-type TE element enhances as the A_n/A_p increases.

Due to the inverse variation of $(T_{1p} - T_{2p})$ and $(T_{1n} - T_{2n})$ with the increment of A_n/A_p, the maximum output power and efficiency have non-monotonic trends according to (6a), (6b) and the classic TE theory [57]. The optimal cross sectional area ratio of the TE elements, $(A_n/A_p)_{opt}$, for maximum output power is shown in Fig. 8(a). With increment of h_h or h_c, the $(A_n/A_p)_{opt}$ increases monotonically. When $h_h \leq 200$ W/K/m^2, the $(A_n/A_p)_{opt}$ is nearly changeless as h_c increases. However, the $(A_n/A_p)_{opt}$ increases significantly with increasing of h_c when $h_h \geq 500$ W/K/m^2.

The optimal $(A_n/A_p)_{opt}$ for maximum efficiency is shown in Fig. 8(b). With the increasing of h_c, $(A_n/A_p)_{opt}$ stays almost constant when h_h is very low (i.e. the case $h_h \leq 200$ W/K/m^2), while it has monotonically increment for the cases of $h_h \geq 500$ W/K/m^2. For arbitrary h_c, the $(A_n/A_p)_{opt}$ increases with increasing of h_h.

V. CONCLUSIONS

A fully coupled analytical model is established to couple internal and external critical design parameters for maximum output power and conversion efficiency. The model contains the main non-identical temperature-dependent material properties. By consideration of a wide range of R_L, h_h, h_c, F and dimensions of TE elements, systematic calculations and analysis were carried out. The results show that, the internal parameters of TE elements are strongly correlated with the external load resistance, and the statistical parameters of TE element present non-linear behaviour. The hot junction temperature of the TE element increases monotonically as R_L increases, while the cold junction temperature decreases. The optimal resistance ratio m_{opt} is greater than unit and it decreases monotonically with the increasing of h_c; while with the increasing of h_h, m_{opt} monotonically increases when $h_c \leq 500$ W/K/m^2, and it has non-monotonic trend for $h_c > 500$ W/K/m^2. Optimal values for h_h/h_c in order to reach maximum output power and conversion efficiency are obtained for fixed $h_h + h_c$. The optimal fill factor F_{opt} for w_{max} can reach unit when h_h and h_c are relatively high. The optimal $(A_n/A_p)_{opt}$ for w_{max} is larger than that for η_{max}, and as h_h or h_c increase the variation of $(A_n/A_p)_{opt}$ for w_{max} and η_{max} becomes very complex.

The proposed model is validated to be accurate and efficient for parametric optimization analysis of TEG. In future work, multi-parameter co-optimization of TEG system will be conducted by applying some intelligent algorithms, e.g. genetic algorithm, particle swarm optimization, and neural network algorithm, etc.

REFERENCES

[1] B. I. Ismail and W. H. Ahmed, "Thermoelectric power generation using waste-heat energy as an alternative green technology," *Recent Patents Elect. Electron. Eng.*, vol. 2, no. 1, pp. 27–39, 2009.

[2] L. E. Bell, "Cooling, heating, generating power, and recovering waste heat with thermoelectric systems," *Science*, vol. 321, pp. 1457–1461, Sep. 2008.

[3] X. Gou, H. Xiao, and S. Yang, "Modeling, experimental study and optimization on low-temperature waste heat thermoelectric generator system," *Appl. Energy*, vol. 87, no. 10, pp. 3131–3136, 2010.

[4] T. J. Hendricks, N. K. Karri, T. P. Hogan, and C. J. Cauchy, "New perspectives in thermoelectric energy recovery system design optimization," *J. Electron. Mater.*, vol. 42, no. 7, pp. 1725–1736, 2013.
[5] S. Wu, H. Zhang, and M. Ni, "Performance assessment of a hybrid system integrating a molten carbonate fuel cell and a thermoelectric generator," *Energy*, vol. 112, pp. 520–527, Oct. 2016.
[6] Y. Wang, S. Su, T. Liu, G. Su, and J. Chen, "Performance evaluation and parametric optimum design of an updated thermionic-thermoelectric generator hybrid system," *Energy*, vol. 90, pp. 1575–1583, Oct. 2015.
[7] A. Montecucco, J. Siviter, and A. R. Knox, "Combined heat and power system for stoves with thermoelectric generators," *Appl. Energy*, vol. 185, pp. 1336–1342, Jan. 2017.
[8] C.-C. Weng and M.-J. Huang, "A simulation study of automotive waste heat recovery using a thermoelectric power generator," *Int. J. Therm. Sci.*, vol. 71, pp. 302–309, Sep. 2013.
[9] Y. Wang, C. Dai, and S. Wang, "Theoretical analysis of a thermoelectric generator using exhaust gas of vehicles as heat source," *Appl. Energy*, vol. 112, pp. 1171–1180, Dec. 2013.
[10] E. F. Sawires, M. I. Eladawy, Y. I. Ismail, and H. Abdelhamid, "Thermal resistance model for standard CMOS thermoelectric generator," *IEEE Access*, vol. 6, pp. 8123–8132, 2018.
[11] S. Qing, A. Alireza, L. A. Rosendahl, A. A. Enkeshafi, and X. Gou, "Characteristics and parametric analysis of a novel flexible ink-based thermoelectric generator for human body sensor," *Energy Convers. Manage.*, vol. 156, pp. 655–665, Jan. 2018.
[12] C. Suter, Z. R. Jovanovic, and A. Steinfeld, "A 1 kW_e thermoelectric stack for geothermal power generation—Modeling and geometrical optimization," *Appl. Energy*, vol. 99, pp. 379–385, Nov. 2012.
[13] S. Mahmoudinezhad, A. Rezania, and L. A. Rosendahl, "Behavior of hybrid concentrated photovoltaic-thermoelectric generator under variable solar radiation," *Energy Convers. Manage.*, vol. 164, pp. 443–452, May 2018.
[14] W.-H. Chen, C.-C. Wang, C.-I. Hung, C.-C. Yang, and R.-C. Juang, "Modeling and simulation for the design of thermal-concentrated solar thermoelectric generator," *Energy*, vol. 64, pp. 287–297, Jan. 2014.
[15] A. Rezania and L. A. Rosendahl, "Feasibility and parametric evaluation of hybrid concentrated photovoltaic-thermoelectric system," *Appl. Energy*, vol. 187, pp. 380–389, Feb. 2017.
[16] R. C. O'Brien, R. M. Ambrosi, N. P. Bannister, S. D. Howe, and H. V. Atkinson, "Safe radioisotope thermoelectric generators and heat sources for space applications," *J. Nucl. Mater.*, vol. 377, no. 3, pp. 506–521, 2008.
[17] R. O. Suzuki and D. Tanaka, "Mathematical simulation of thermoelectric power generation with the multi-panels," *J. Power Sources*, vol. 122, no. 2, pp. 201–209, 2003.
[18] J. Yu and H. Zhao, "A numerical model for thermoelectric generator with the parallel-plate heat exchanger," *J. Power Sources*, vol. 172, no. 1, pp. 428–434, 2007.
[19] S. Kim, "Analysis and modeling of effective temperature differences and electrical parameters of thermoelectric generators," *Appl. Energy*, vol. 102, pp. 1458–1463, Feb. 2013.
[20] X. Liang, X. Sun, H. Tian, G. Shu, Y. Wang, and X. Wang, "Comparison and parameter optimization of a two-stage thermoelectric generator using high temperature exhaust of internal combustion engine," *Appl. Energy*, vol. 130, pp. 190–199, Oct. 2014.
[21] G. Liang, J. Zhou, and X. Huang, "Analytical model of parallel thermoelectric generator," *Appl. Energy*, vol. 88, no. 12, pp. 5193–5199, 2011.
[22] X. Meng and R. O. Suzuki, "Helical configuration for thermoelectric generation," *Appl. Therm. Eng.*, vol. 99, pp. 352–357, Apr. 2016.
[23] X. Jia and Y. Gao, "Optimal design of a novel thermoelectric generator with linear-shaped structure under different operating temperature conditions," *Appl. Therm. Eng.*, vol. 78, pp. 533–542, Mar. 2015.
[24] D. M. Rowe and G. Min, "Evaluation of thermoelectric modules for power generation," *J. Power Sources*, vol. 73, no. 2, pp. 193–198, Jun. 1998.
[25] B. S. Yilbas and A. Z. Sahin, "Thermoelectric device and optimum external load parameter and slenderness ratio," *Energy*, vol. 35, no. 12, pp. 5380–5384, 2010.
[26] K. Yazawa and A. Shakouri, "Optimization of power and efficiency of thermoelectric devices with asymmetric thermal contacts," *J. Appl. Phys.*, vol. 111, no. 2, p. 024509, 2012.
[27] K. Yazawa and A. Shakouri, "Cost-efficiency trade-off and the design of thermoelectric power generators," *Environ. Sci. Technol.*, vol. 45, no. 17, pp. 7548–7553, 2011.
[28] A. Rezania, K. Yazawa, L. A. Rosendahl, and A. Shakouri, "Co-optimized design of microchannel heat exchangers and thermoelectric generators," *Int. J. Therm. Sci.*, vol. 72, pp. 73–81, Oct. 2013.
[29] J.-Y. Jang, Y.-C. Tsai, and C.-W. Wu, "A study of 3-D numerical simulation and comparison with experimental results on turbulent flow of venting flue gas using thermoelectric generator modules and plate fin heat sink," *Energy*, vol. 53, pp. 270–281, May 2013.
[30] A. Rezania and L. A. Rosendahl, "Evaluating thermoelectric power generation device performance using a rectangular microchannel heat sink," *J. Electron. Mater.*, vol. 40, no. 5, pp. 481–488, 2011.
[31] Y. Shi, Z. Zhu, Y. Deng, W. Zhu, X. Chen, and Y. Zhao, "A real-sized three-dimensional numerical model of thermoelectric generators at a given thermal input and matched load resistance," *Energy Convers. Manage.*, vol. 101, pp. 713–720, Sep. 2015.
[32] A. Rezania and L. A. Rosendahl, "A comparison of micro-structured flat-plate and cross-cut heat sinks for thermoelectric generation application," *Energy Convers. Manage.*, vol. 101, pp. 730–737, Sep. 2015.
[33] J.-H. Meng, X.-X. Zhang, and X.-D. Wang, "Characteristics analysis and parametric study of a thermoelectric generator by considering variable material properties and heat losses," *Int. J. Heat Mass Transf.*, vol. 80, pp. 227–235, Jan. 2015.
[34] Y. Wang *et al.*, "Nb-doped grain boundary induced thermoelectric power factor enhancement in La-doped $SrTiO_3$ nanoceramics," *J. Power Sources*, vol. 241, pp. 255–258, Nov. 2013.
[35] T. Zhang, "New thinking on modeling of thermoelectric devices," *Appl. Energy*, vol. 168, pp. 65–74, Apr. 2016.
[36] M. M. Barry, K. A. Agbim, P. Rao, C. E. Clifford, B. V. K. Reddy, and M. K. Chyu, "Geometric optimization of thermoelectric elements for maximum efficiency and power output," *Energy*, vol. 112, pp. 388–407, Oct. 2016.
[37] Z.-G. Shen, S.-Y. Wu, L. Xiao, and G. Yin, "Theoretical modeling of thermoelectric generator with particular emphasis on the effect of side surface heat transfer," *Energy*, vol. 95, pp. 367–379, Jun. 2016.
[38] S. Manikandan and S. C. Kaushik, "The influence of Thomson effect in the performance optimization of a two stage thermoelectric generator," *Energy*, vol. 100, pp. 227–237, Apr. 2016.
[39] Y. Feng, L. Chen, F. Meng, and F. Sun, "Influences of the thomson effect on the performance of a thermoelectric generator-driven thermoelectric heat pump combined device," *Entropy*, vol. 20, no. 1, p. 29, 2018.
[40] Y. Feng, L. Chen, F. Meng, and F. Sun, "Thermodynamic analysis of TEG-TEC device including influence of thomson effect," *J. Non-Equilibrium Thermodynamics*, vol. 43, no. 1, pp. 75–86, 2018.
[41] Y. J. Wu, L. Zuo, J. Chen, and J. A. Klein, "A model to analyze the device level performance of thermoelectric generator," *Energy*, vol. 115, pp. 591–603, Nov. 2016.
[42] M. Chen, L. A. Rosendahl, T. J. Condra, and J. K. Pedersen, "Numerical modeling of thermoelectric generators with varing material properties in a circuit simulator," *IEEE Trans. Energy Convers.*, vol. 24, no. 1, pp. 112–124, Mar. 2009.
[43] M. Chen, L. A. Rosendahl, and T. Condra, "A three-dimensional numerical model of thermoelectric generators in fluid power systems," *Int. J. Heat Mass Transf.*, vol. 54, nos. 1–3, pp. 345–355, 2011.
[44] A. Rezania and L. A. Rosendahl, "New configurations of micro plate-fin heat sink to reduce coolant pumping power," *J. Electron. Mater.*, vol. 41, no. 6, pp. 1298–1304, 2012.
[45] A. Rezania, L. A. Rosendahl, and H. Yin, "Parametric optimization of thermoelectric elements footprint for maximum power generation," *J. Power Sources*, vol. 255, pp. 151–156, Jun. 2014.
[46] J.-H. Meng, X.-X. Zhang, and X.-D. Wang, "Multi-objective and multi-parameter optimization of a thermoelectric generator module," *Energy*, vol. 71, pp. 367–376, Jul. 2014.
[47] Z. Niu *et al.*, "Elucidating modeling aspects of thermoelectric generator," *Int. J. Heat Mass Transf.*, vol. 85, pp. 12–32, Jun. 2015.
[48] U. Erturun, K. Erermis, and K. Mossi, "Influence of leg sizing and spacing on power generation and thermal stresses of thermoelectric devices," *Appl. Energy*, vol. 159, pp. 19–27, Dec. 2015.
[49] O. Högblom and R. Andersson, "A simulation framework for prediction of thermoelectric generator system performance," *Appl. Energy*, vol. 180, pp. 472–482, Oct. 2016.
[50] A. Montecucco and A. R. Knox, "Maximum power point tracking converter based on the open-circuit voltage method for thermoelectric generators," *IEEE Trans. Power Electron.*, vol. 30, no. 2, pp. 828–839, Feb. 2015.

[51] B. Vermeersch and G. De Mey, "A fixed-angle dynamic heat spreading model for (An) isotropic rear-cooled substrates," *ASME J. Heat Transf.*, vol. 130, no. 12, p. 121301, 2008.
[52] H. Yin, S. Johnsen, K. A. Borup, K. Kato, M. Takatac, and B. B. Iversen, "Highly enhanced thermal stability of Zn_4Sb_3 nanocomposites," *Chem. Commun.*, vol. 49, no. 58, pp. 6540–6542, 2013.
[53] M. SØndergaard, M. Christensen, K. A. Borup, H. Yin, and B. B. Iversen, "Gravity-induced gradients in thermoelectric $Mg_2Si_{0.9925-x}Sn_xSb_{0.0075}$," *Acta Mater.*, vol. 60, no. 16, pp. 5745–5751, 2012.
[54] S. LeBlanc, S. K. Yee, M. L. Scullin, C. Dames, and K. E. Goodson, "Material and manufacturing cost considerations for thermoelectrics," *Renew. Sustain. Energy Rev.*, vol. 32, pp. 313–327, Apr. 2014.
[55] S. K. Yee, S. LeBlanc, K. E. Goodson, and C. Dames, "$ per W metrics for thermoelectric power generation: Beyond ZT," *Energy Environ. Sci.*, vol. 6, no. 9, pp. 2561–2571, 2013.
[56] T. J. Hendricks, S. Yee, and S. LeBlanc, "Cost scaling of a real-world exhaust waste heat recovery thermoelectric generator: A deeper dive," *J. Electron. Mater.*, vol. 45, no. 3, pp. 1751–1761, 2015.
[57] D. M. Rowe, *Modules, Systems, and Applications in Thermoelectrics*. Boca Raton, FL, USA: CRC Press, 2012.

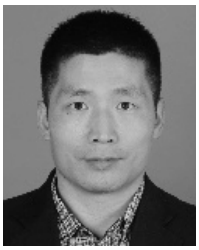

SHAOWEI QING was born in Jianyang, Sichuan, China, in 1981. He received the master's and Ph.D. degrees in power machinery and engineering from the Harbin Institute of Technology, Harbin, in 2007 and 2012, respectively. He was a Guest Researcher with the Institute of Energy Technology, Aalborg University, Aalborg, Denmark, from 2016 to 2017. He is currently a Lecturer with the Institute of Energy and Power Engineering, Chongqing University, Chongqing. His current research interests include modeling of thermoelectric devices for power/energy systems, thermoelectric energy harvesting, development and design of application-based prototypes, and testing and measurement techniques.

ALIREZA REZANIAKOLAEI received the Ph.D. degree from Aalborg University in 2012. He is currently an Associate Professor of energy technologies with Aalborg University. He is also the Head of the Low Power Energy Harvesting & i-Solutions Research Programme at ET with 10 years experiences in this field. His current research interests include fluid mechanics, thermal engineering and energy harvesting technologies, micro heat transfer surfaces and integration of these technologies with renewable systems, actuators, and sensor applications.

LASSE A. ROSENDAHL was born in Ribe, Denmark, in 1967. He received the M.Sc. and Ph.D. degrees in mechanical engineering from Aalborg University, Aalborg, Denmark. From 1998 to 1999, he was with the Department of Energy Technology, Aalborg University, as an Assistant Professor, and as an Associate Professor from 2000 to 2007. In 1999, he was employed with Research and Development Department, Grundfos A/S. He has been a Professor with Aalborg University since 2007. He is currently a Leader of Biomass Research Programme at IET. His current research interests include fluid mechanics, thermal energy technology, liquid biofuels, and novel energy technologies, including modeling, simulation, and design with a focus on optimized efficiency.

XIAOLONG GOU was born in Sichuan, China, in 1972. He received the master's and Ph.D. degrees with the Institute of Power Engineering, Chongqing University, Chongqing, China, in 1998 and 2003, respectively. He was a Visiting Scholar with Princeton University from 2008 to 2009. He has been a Professor with the Institute of Power Engineering, Chongqing University, since 2010. His current research interests include combustion science and technology, and modeling and controlling optimization of thermal power systems.